Optics Communications 466 (2020) 125655

Contents lists available at ScienceDirect

Optics Communications

journal homepage: www.elsevier.com/locate/optcom

# Experimental demonstration of quantum interference modulation via precise dephasing control in atoms

Jinhong Liu [a,b], Jinze Wu [a,b,*], Yaodong Hu [b], Yu Zhang [b], Junxiang Zhang [a,b,*]

[a] State Key Laboratory of Quantum Optics and Quantum Optics Devices, Institute of Opto-Electronics, and Collaborative Innovation Center of Extreme Optics, Shanxi University, Taiyuan 030006, China

[b] Interdisciplinary Center of Quantum Information, State Key Laboratory of Modern Optical Instrumentation, and Zhejiang Province Key Laboratory of Quantum Technology and Device of Physics Department, Zhejiang University, Hangzhou 310027, China

ARTICLE INFO

*Keywords:*
Quantum interference
Dephasing
Electromagnetically induced transparency
Autler–Townes splitting

ABSTRACT

We theoretically and experimentally demonstrate the manipulation of quantum interference in atom-field systems via dephasing, which can be precisely and selectively controlled by phase-diffusion induced dephasing of interacting fields. The continuous control of quantum interference from destructive interference (suppression of absorption) to constructive interference (enhancement of absorption) can be obtained by changing the dephasing rate. Our work highlights the key role of dephasing in intentionally manipulation of quantum interference for tunable delay and storage of broadband pulses.

## 1. Introduction

Quantum interference [1–4] in multilevel atomic systems is an important effect in quantum optics and leads to many fascinating phenomena. One of the most well-known phenomena is electromagnetically induced transparency (EIT) [5–8], in which quantum interference between different excitation pathways leads to a narrow transparency window accompanied by an extremely steep dispersion [9]. Owing to these features, EIT has important applications in light storage and quantum memories [10–13], non-classical light preparations [14–17], all-optical devices [18–20], etc. EIT has also been recognized as a general technique to be employed in other systems, such as optomechanical systems [21], quantum dots [22], superconducting circuits [23], nanoplasmonics [24], etc., allowing the realization of integral components for quantum communication [25] and computation [26].

In general, EIT is a joint effect of quantum interference and Autler–Townes splitting (ATS) [27–29], which originates from the splitting of two dressed states created by a coupling field. When the Rabi frequency of the coupling field is less than or comparable to atomic decay rates, the two dressed states are close to each other, giving rise to strong quantum interference for the narrow transparency window, i.e., EIT. When the Rabi frequency of the coupling field is much stronger than atomic decay rates, the well separated dressed states make the quantum interference negligible. As a result, a wide transparency window appears due to the simple superposition of two Lorentzian absorption profiles. The relative weights of EIT and ATS in various systems keep an active topic of research [30–36]. Very recently, ATS has been employed to realize high-speed broadband quantum memory by controlling the Rabi frequency of the coupling field in an atomic system [37].

Apart from the modification of quantum interference via the Rabi frequency of the coupling field, the dephasing rate also plays a role on quantum interference, but receives relatively little attention. Generally, the dephasing, arising from the coupling of atoms with environment such as atom–atom and atom–wall collisions [38,39], is regarded as an unfavorable factor since it may destroy the atomic coherence (decoherence) [5,37].

In this article, we theoretically and experimentally show that the precise control of dephasing can lead to the transition between destructive quantum interference (suppressed absorption, i.e., EIT) and constructive quantum interference (enhanced absorption) in two kinds of atomic systems: EIT- and ATS-type systems. Theoretically, we use the phase-diffusion model to show that the phase diffusion rates (linewidths) of interacting fields play a crucial role in manipulation of the dephasing rates in atoms, and we then present the experiment via field induced dephasing to verify the theoretical results, showing that this method is much more feasible and precise. Dynamical control of the quantum interference via dephasing may find applications in optical manipulation, such as spectral–temporal pulse shaping, temporal beam splitting, and optical storage for broadband networks. Joint control of the Rabi frequency and the dephasing rate makes it possible to realize multidimensional light manipulations.

* Corresponding authors.
*E-mail addresses:* wujinze_qc@sina.cn (J. Wu), junxiang_zhang@zju.edu.cn (J. Zhang).

https://doi.org/10.1016/j.optcom.2020.125655
Received 24 December 2019; Received in revised form 17 February 2020; Accepted 29 February 2020
Available online 3 March 2020

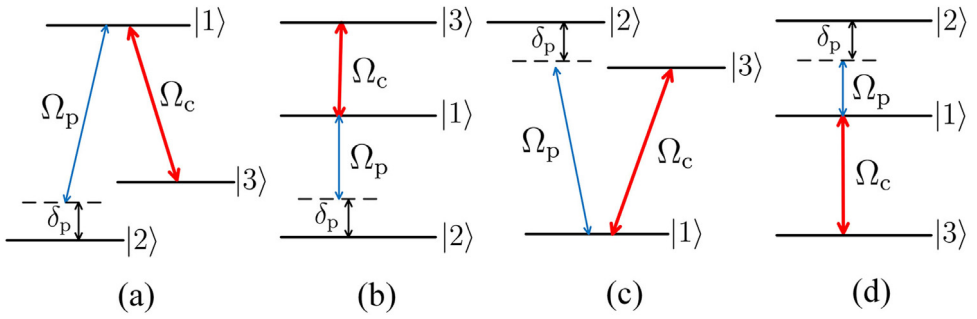


**Fig. 1.** Three-level systems in $^{133}$Cs atoms. (a) $\Lambda$-type system with $|1\rangle = |6P_{1/2}, F' = 4\rangle$, $|2\rangle = |6S_{1/2}, F = 3\rangle$, and $|3\rangle = |6S_{1/2}, F = 4\rangle$; (b) UC-type system with $|1\rangle = |6P_{3/2}, F' = 5\rangle$, $|2\rangle = |6S_{1/2}, F = 4\rangle$, and $|3\rangle = |6D_{3/2}, F'' = 5\rangle$; (c) V-type system with $|1\rangle = |6S_{1/2}, F = 3\rangle$, $|2\rangle = |6P_{1/2}, F' = 4\rangle$, and $|3\rangle = |6P_{1/2}, F' = 3\rangle$; (d) LC-type system with $|1\rangle = |6P_{3/2}, F' = 5\rangle$, $|2\rangle = |6D_{3/2}, F'' = 5\rangle$, and $|3\rangle = |6S_{1/2}, F = 4\rangle$.

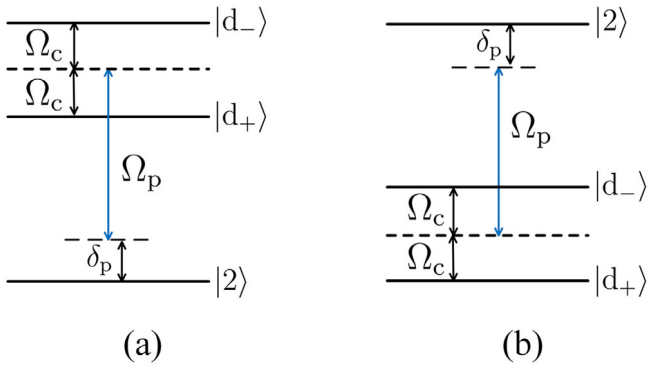


**Fig. 2.** Dressed-state representation for (a) $\Lambda$- and UC- type systems, and (b) V- and LC-type systems.

## 2. Theory

We consider four types of three-level systems in $^{133}$Cs atoms: $\Lambda$-, upper-cascade (UC)-, V-, and lower-cascade (LC)-type systems depicted in Fig. 1(a), (b), (c), and (d), respectively. Each system is driven by a strong coupling field $E_c = \mathcal{E}_c e^{-i\nu_c t}$ resonantly on the transition $|1\rangle \leftrightarrow |3\rangle$ and probed by a weak probe field $E_p = \mathcal{E}_p e^{-i\nu_p t}$ scanning across the transition $|1\rangle \leftrightarrow |2\rangle$. Here $\mathcal{E}_{c(p)}$ and $\nu_{c(p)}$ are the amplitude and angular frequency of the coupling (probe) field.

In the presence of the coupling field, the state $|1\rangle$ is splitted into two dressed states $|d_+\rangle$ and $|d_-\rangle$ due to ATS. For $\Lambda$- and UC-type systems one has two upper dressed states [see Fig. 2(a)], and for V- and LC-type systems one has two lower dressed states [see Fig. 2(b)]. Quantum interference occurs between the two transitions $|d_+\rangle \leftrightarrow |2\rangle$ and $|d_-\rangle \leftrightarrow |2\rangle$.

### 2.1. $\Lambda$- and UC-type systems

For $\Lambda$- and UC-type systems [see Figs. 1(a), (b), and 2(a)], the probe absorption is proportional to the imaginary part of the susceptibility given by

$$\chi \propto \frac{1}{\sqrt{2}}(\rho_{d_+2} + \rho_{d_-2}), \tag{1}$$

where $\rho_{d_\pm 2}$ is the density matrix element representing the atomic coherence between $|d_\pm\rangle$ and $|2\rangle$, and satisfies

$$\dot{\rho}_{d_+2} = -[i(\delta_p - \Omega_c) + \gamma_d]\rho_{d_+2} - \eta\rho_{d_-2} + \frac{i\Omega_p}{\sqrt{2}}(\rho_{22} - \rho_{d_+d_+} - \rho_{d_+d_-}), \tag{2a}$$

$$\dot{\rho}_{d_-2} = -[i(\delta_p + \Omega_c) + \gamma_d]\rho_{d_-2} - \eta\rho_{d_+2} + \frac{i\Omega_p}{\sqrt{2}}(\rho_{22} - \rho_{d_-d_-} - \rho_{d_-d_+}). \tag{2b}$$

Here $\delta_p = \omega_{12} - \nu_p$ is the probe detuning, $\omega_{12}$ is the resonant frequency of the transition $|1\rangle \leftrightarrow |2\rangle$; $\Omega_{c(p)} = \mathcal{E}_{c(p)} d_{13(12)}/\hbar$ is the Rabi frequency of the coupling (probe) field, $d_{13(12)}$ is the dipole moment matrix element of the transition $|1\rangle \leftrightarrow |3\rangle (|1\rangle \leftrightarrow |2\rangle)$. $\gamma_d = (\gamma_{12} + \gamma_{23})/2$ represents the decay rate of $\rho_{d_\pm 2}$, where $\gamma_{ij}$ $(i, j = 1, 2, 3)$ is the decay rate of the off-diagonal density matrix element $\rho_{ij}$.

For $\Lambda$-type system, one has $\gamma_{12} = (\Gamma_{12} + \Gamma_{13})/2 + \gamma_{12}^{(d)}$, $\gamma_{13} = (\Gamma_{12} + \Gamma_{13})/2 + \gamma_{13}^{(d)}$, and $\gamma_{23} = \gamma_{23}^{(d)}$. For UC-type system, one has $\gamma_{12} = \Gamma_{12}/2 + \gamma_{12}^{(d)}$, $\gamma_{13} = (\Gamma_{31} + \Gamma_{12})/2 + \gamma_{13}^{(d)}$, and $\gamma_{23} = \Gamma_{31}/2 + \gamma_{23}^{(d)}$. Here $\Gamma_{ij}$ is the spontaneous decay rate from $|i\rangle$ to $|j\rangle$, and $\gamma_{ij}^{(d)}$ is the dephasing rate of $\rho_{ij}$.

It can be seen from Eqs. (2) that $\rho_{d_+2}$ and $\rho_{d_-2}$ are coupled to each other by the parameter $\eta = (\gamma_{12} - \gamma_{23})/2$, and are independent when $\eta = 0$. It means that the quantum interference between the transitions $|d_+\rangle \leftrightarrow |2\rangle$ and $|d_-\rangle \leftrightarrow |2\rangle$ is determined by $\eta$, which depends on the spontaneous decay rate and the dephasing rate:

$$\eta = \frac{\Gamma_{12} + \Gamma_{13}}{4} + \frac{\gamma_{12}^{(d)} - \gamma_{23}^{(d)}}{2}, \qquad \Lambda - \text{type}, \tag{3a}$$

$$\eta = \frac{\Gamma_{12} - \Gamma_{31}}{4} + \frac{\gamma_{12}^{(d)} - \gamma_{23}^{(d)}}{2}, \qquad \text{UC} - \text{type}. \tag{3b}$$

We solve Eqs. (2) (up to the first order of $\Omega_p$) and substitute the solutions into Eq. (1) to obtain the probe absorption:

$$\text{Im}\chi \propto \frac{\gamma_d}{(\delta_p - \Omega_c)^2 + \gamma_d^2} + \frac{\gamma_d}{(\delta_p + \Omega_c)^2 + \gamma_d^2} + \Phi, \tag{4}$$

with

$$\Phi = -\eta \text{Re}\frac{2[(i\delta_p + \gamma_d)(i\delta_p + \gamma_d - \eta) + \Omega_c^2]}{[(i\delta_p + \gamma_d)^2 + \Omega_c^2][(i\delta_p + \gamma_d)^2 - \eta^2 + \Omega_c^2]}. \tag{5}$$

Figs. 3 ($\Lambda$-type system) and 4 (UC-type system) plot the probe absorption spectra in the cases of $\eta = 0$, $\eta > 0$, and $\eta < 0$. The value of $\eta$ is modified by changing the dephasing rate $\gamma_{23}^{(d)}$. If $\eta = 0$ [Figs. 3(a) and 4(a)], one has $\Phi = 0$ and thus the absorption (orange solid line) is simply a superposition of two separated Lorentzian absorption profiles (gray dotted lines) given by the first two terms in Eq. (4), which is characterized as ATS [27,28]. For $\eta > 0$ [Figs. 3(b) and 4(b)], one has $\Phi < 0$ and thus the absorption (orange solid line) is suppressed at $\delta_p = 0$ relative to the ATS case (black dashed line), i.e., the destructive quantum interference (EIT). For $\eta < 0$ [Figs. 3(c) and 4(c)], one has $\Phi > 0$ and thus the absorption is enhanced relative to the ATS case, i.e., the constructive quantum interference. Therefore, $\eta$ is responsible for the quantum interference and the sign of $\eta$ determines the type of the quantum interference.

Fig. 5 plots the absorption spectra for the cases of weak and strong coupling fields with $\eta > 0$ (destructive interference). For a weak coupling field ($\Omega_c < \gamma_d$), the destructive quantum interference can create a narrow transparency window, as shown in Fig. 5(a) and (c). Owing to this feature, the $\Lambda$- and UC-type systems are usually employed

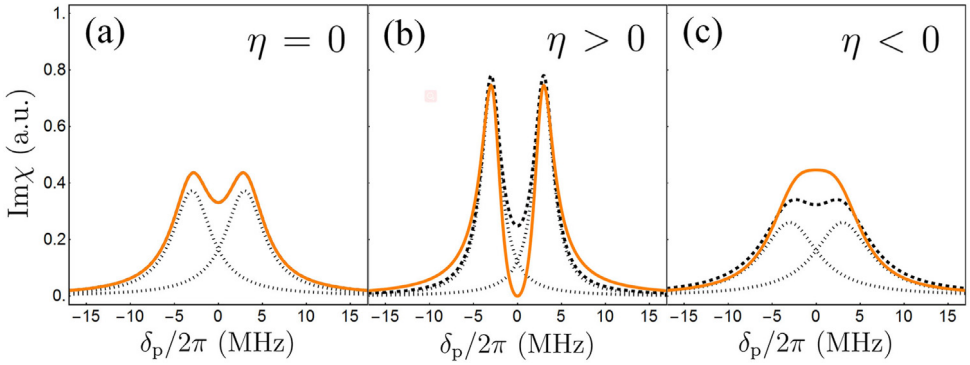


**Fig. 3.** Probe absorption spectra (orange solid lines) for $\Lambda$-type system with (a) $\eta = 0$ ($\gamma_{23}^{(d)} = 2\pi \times 2.69$ MHz); (b) $\eta = 2\pi \times 1.34$ MHz ($\gamma_{23}^{(d)} = 0$); (c) $\eta = -2\pi \times 1.16$ MHz ($\gamma_{23}^{(d)} = 2\pi \times 5$ MHz). The other parameters are: $\Gamma_{12} = 2\pi \times 3.45$ MHz, $\Gamma_{13} = 2\pi \times 1.92$ MHz, $\gamma_{12}^{(d)} = 0$, and $\Omega_c = 2\pi \times 3$ MHz. The gray dotted lines are the two Lorentzian absorption profiles, and the black dashed lines are their summation corresponding to ATS.

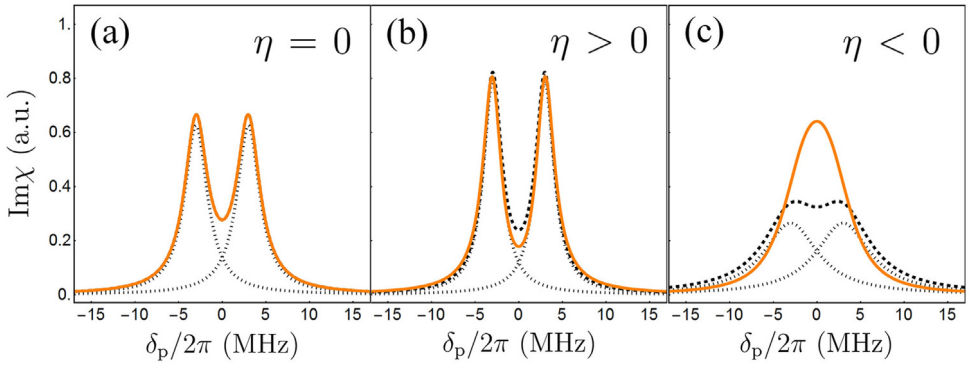


**Fig. 4.** Probe absorption spectra (orange solid lines) for UC-type system with (a) $\eta = 0$ ($\gamma_{23}^{(d)} = 2\pi \times 0.67$ MHz); (b) $\eta = 2\pi \times 0.33$ MHz ($\gamma_{23}^{(d)} = 0$); (c) $\eta = -2\pi \times 2.17$ MHz ($\gamma_{23}^{(d)} = 2\pi \times 5$ MHz). The other parameters are: $\Gamma_{12} = 2\pi \times 3.20$ MHz, $\Gamma_{31} = 2\pi \times 1.87$ MHz, $\gamma_{12}^{(d)} = 0$, and $\Omega_c = 2\pi \times 3$ MHz.

to demonstrate EIT, and they are classified as EIT-type system [40,41]. On the other hand, when the coupling field is strong, the quantum interference is weak and the large ATS gives rise to a wide transparency window, as shown in Fig. 5(b) and (d). In this case, large $\Omega_c$ results in well separated dressed states $|d_\pm\rangle$, and the two transitions $|d_+\rangle \leftrightarrow |2\rangle$ and $|d_-\rangle \leftrightarrow |2\rangle$ are hardly coupled to the same field mode, making the quantum interference negligible [2,3].

### 2.2. V- and LC-type systems

For V- and LC-type systems, the susceptibility is given by

$$\chi \propto \frac{1}{\sqrt{2}}(\rho_{2d_+} + \rho_{2d_-}), \tag{6}$$

with $\rho_{2d_+}$ and $\rho_{2d_-}$ satisfying

$$\dot{\rho}_{2d_+} = -[i(\delta_p + \Omega_c) + \gamma_d]\rho_{2d_+} - \eta\rho_{2d_-} + \frac{i\Omega_p}{\sqrt{2}}(\rho_{d_+d_+} + \rho_{d_-d_+} - \rho_{22}), \tag{7a}$$

$$\dot{\rho}_{2d_-} = -[i(\delta_p - \Omega_c) + \gamma_d]\rho_{2d_-} - \eta\rho_{2d_+} + \frac{i\Omega_p}{\sqrt{2}}(\rho_{d_-d_-} + \rho_{d_+d_-} - \rho_{22}), \tag{7b}$$

where $\delta_p$, $\Omega_{c(p)}$, $\gamma_d$, and $\eta$ have the same definitions as in Eqs. (2).

It is seen from Eqs. (7) that $\rho_{2d_+}$ and $\rho_{2d_-}$ are also coupled to each other by $\eta$, and thus $\eta$ is responsible for the quantum interference between the transitions $|d_+\rangle \leftrightarrow |2\rangle$ and $|d_-\rangle \leftrightarrow |2\rangle$. For V- and LC- type systems, $\eta$ is given by

$$\eta = -\frac{\Gamma_{31}}{4} + \frac{\gamma_{12}^{(d)} - \gamma_{23}^{(d)}}{2}, \qquad V - \text{type}, \tag{8a}$$

$$\eta = \frac{\Gamma_{13}}{4} + \frac{\gamma_{12}^{(d)} - \gamma_{23}^{(d)}}{2}, \qquad LC - \text{type}. \tag{8b}$$

The probe absorption is obtained by solving Eqs. (7):

$$\begin{aligned} \mathrm{Im}\chi \propto & \frac{(1/2 + \mathrm{Re}\rho_{d_+d_-})\gamma_d}{(\delta_p - \Omega_c)^2 + \gamma_d^2} + \frac{(1/2 + \mathrm{Re}\rho_{d_+d_-})\gamma_d}{(\delta_p + \Omega_c)^2 + \gamma_d^2} \\ & + \frac{\mathrm{Im}\rho_{d_+d_-}(\delta_p - \Omega_c)}{(\delta_p - \Omega_c)^2 + \gamma_d^2} - \frac{\mathrm{Im}\rho_{d_+d_-}(\delta_p + \Omega_c)}{(\delta_p + \Omega_c)^2 + \gamma_d^2} + \Phi, \end{aligned} \tag{9}$$

with

$$\Phi = -\eta\mathrm{Re}\frac{(1 + 2\mathrm{Re}\rho_{d_+d_-})[(i\delta_p + \gamma_d)(i\delta_p + \gamma_d - \eta) + \Omega_c^2] + 2\mathrm{Im}\rho_{d_+d_-}\eta\Omega_c}{[(i\delta_p + \gamma_d)^2 + \Omega_c^2][(i\delta_p + \gamma_d)^2 - \eta^2 + \Omega_c^2]}, \tag{10}$$

where $\rho_{d_+d_+} = \rho_{d_-d_-} = 1/2$, $\rho_{d_+d_-} = \frac{\Gamma_{31}\gamma_{13}/2 + i\Gamma_{31}\Omega_c}{\Gamma_{31}\gamma_{13} + 4\Omega_c^2}$ for V-type system, and $\rho_{d_+d_-} = -\frac{\Gamma_{13}\gamma_{13}/2 + i\Gamma_{13}\Omega_c}{\Gamma_{13}\gamma_{13} + 4\Omega_c^2}$ for LC-type system.

It is seen from Eq. (9) that the first four terms are independent of $\eta$, and thus represent the absorption without quantum interference. Only the last term $\Phi$ contributes the quantum interference. Fig. 6 plots the probe absorption spectra for V-type system with different values of $\eta$ which is always negative, meaning that only constructive interference can occur. For LC-type system, one can have $\eta = 0$, $\eta > 0$, and $\eta < 0$, corresponding to no interference, destructive interference, and constructive interference, as shown in Fig. 7.

Furthermore, we show the absorption spectra for V- and LC-type systems at weak [Fig. 8(a), (c)] and strong [Fig. 8(b), (d)] coupling fields. For V-type system with a weak coupling field [Fig. 8(a)], the total absorption (orange line) contributed by the first four terms and the last interference term is larger than the absorption without interference (black dashed line) contributed by the first four terms, i.e., the constructive quantum interference. On the other hand, for LC-type system with a weak coupling field [Fig. 8(c)], although the total absorption is weaker

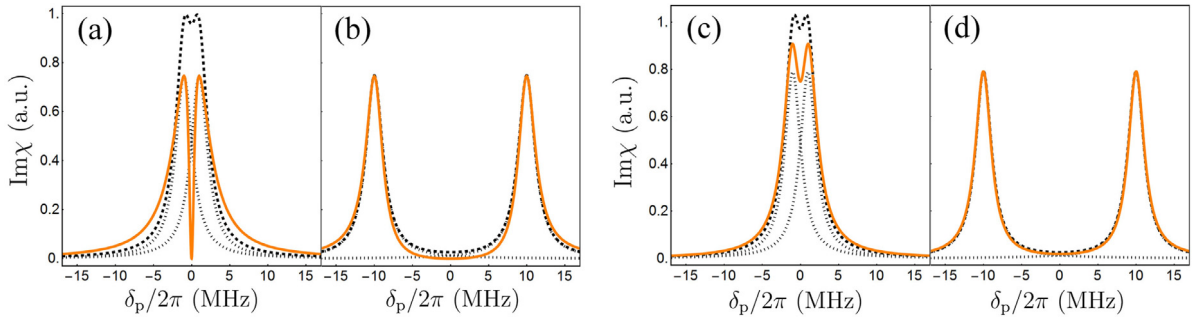


**Fig. 5.** Probe absorption spectra (orange solid lines) of (a), (b) $\Lambda$- and (c), (d) UC-type systems with $\gamma_{23}^{(d)} = 0$ and (a), (c) $\Omega_c = 2\pi \times 1$ MHz; (b), (d) $\Omega_c = 2\pi \times 10$ MHz. The other parameters for $\Lambda$- and UC-type systems are as in Figs. 3 and 4, respectively.

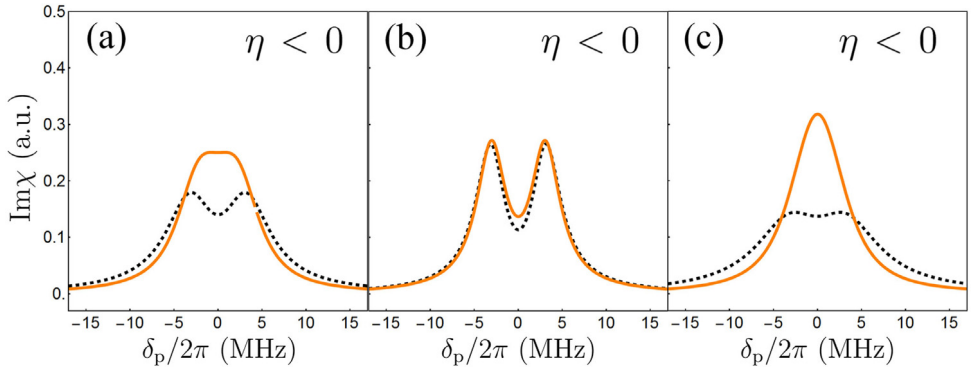


**Fig. 6.** Probe absorption spectra (orange solid lines) for V-type system with (a) $\eta = -2\pi \times 1.54$ MHz ($\gamma_{23}^{(d)} = 2\pi \times 2.5$ MHz); (b) $\eta = -2\pi \times 0.29$ MHz ($\gamma_{23}^{(d)} = 0$); (c) $\eta = -2\pi \times 2.79$ MHz ($\gamma_{23}^{(d)} = 2\pi \times 5$ MHz). The other parameters are: $\Gamma_{21} = 2\pi \times 3.45$ MHz, $\Gamma_{31} = 2\pi \times 1.15$ MHz, $\gamma_{12}^{(d)} = 0$, and $\Omega_c = 2\pi \times 3$ MHz. The black dashed lines are the summation of the first four terms in Eq. (9) without quantum interference.

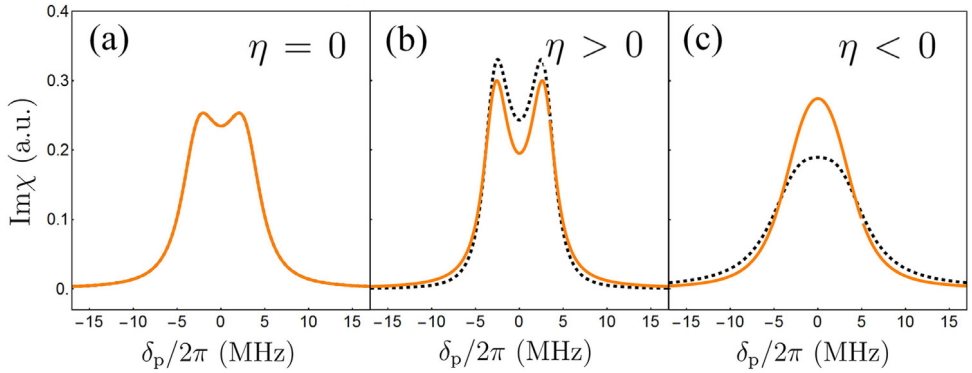


**Fig. 7.** Probe absorption spectra (orange solid lines) for LC-type system with (a) $\eta = 0$ ($\gamma_{23}^{(d)} = 2\pi \times 1.60$ MHz); (b) $\eta = 2\pi \times 0.80$ MHz ($\gamma_{23}^{(d)} = 0$); (c) $\eta = -2\pi \times 1.70$ MHz ($\gamma_{23}^{(d)} = 2\pi \times 5$ MHz). The other parameters are: $\Gamma_{21} = 2\pi \times 1.87$ MHz, $\Gamma_{13} = 2\pi \times 3.20$ MHz, $\gamma_{12}^{(d)} = 0$, and $\Omega_c = 2\pi \times 3$ MHz.

than the absorption without interference, the quantum interference is too weak to create a transparency window. For the case of strong coupling field, the absorption is mainly determined by ATS, as shown in Fig. 8(b) and (d).

The discussion about Fig. 8 tells us the fact that there is almost no transparency window for V- and LC-type systems at weak coupling field. Therefore, the two systems are normally categorized as ATS-type systems [40,41].

### 2.3. Manipulation of atomic dephasing via the phase diffusion of interacting fields

As analyzed in Sections 2.1 and 2.2, the quantum interference can be manipulated by adjusting the dephasing rates $\gamma_{12}^{(d)}$ and $\gamma_{23}^{(d)}$. In general, atomic dephasing arises from the atomic collisions, and the dephasing rate can be adjusted by changing the partial pressure of the buffer gas filled in the atomic vapor [38,39]. However, it is difficult for this method to get the exact value of $\gamma_{12(23)}^{(d)}$ and to only change $\gamma_{12(23)}^{(d)}$ while keeping $\gamma_{23(12)}^{(d)}$ unchanged. Here we show that the phase fluctuations of interacting fields can lead to the atomic dephasing, and the dephasing rates can be precisely and selectively adjusted by controlling the linewidths of the fields.

In general, both the amplitude $\mathcal{E}_{c(p)}$ and phase $\phi_{c(p)}$ of the field exhibit random fluctuations due to the spontaneous emission in the gain medium of a laser. However, if the laser is operating sufficiently far above threshold, the amplitude fluctuation can be ignored, and the field can be described by the phase diffusion model [42]. In this model, the field has a stable amplitude $\mathcal{E}_{c(p)}$ and a random phase $\phi_{c(p)}(t)$:

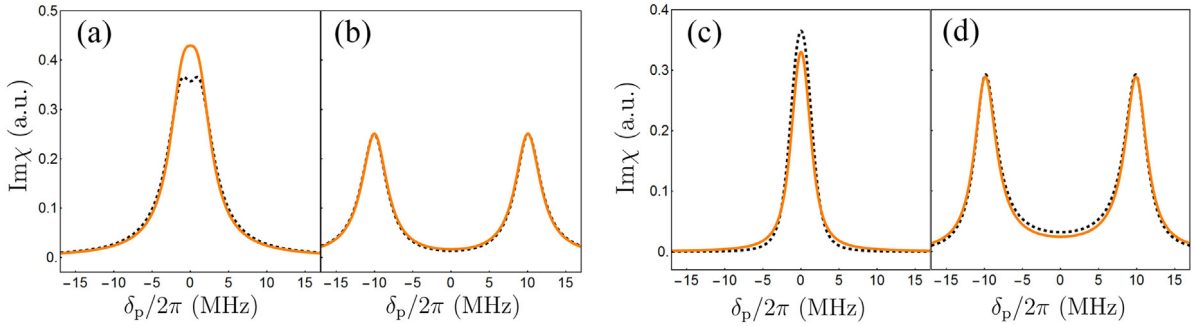


**Fig. 8.** Probe absorption spectra (orange solid lines) of (a), (b) V- and (c), (d) LC-type systems with $\gamma_{23}^{(d)} = 0$ and (a), (c) $\Omega_c = 2\pi \times 1$ MHz; (b), (d) $\Omega_c = 2\pi \times 10$ MHz. The other parameters for V- and LC-type systems are as in Figs. 6 and 7, respectively.

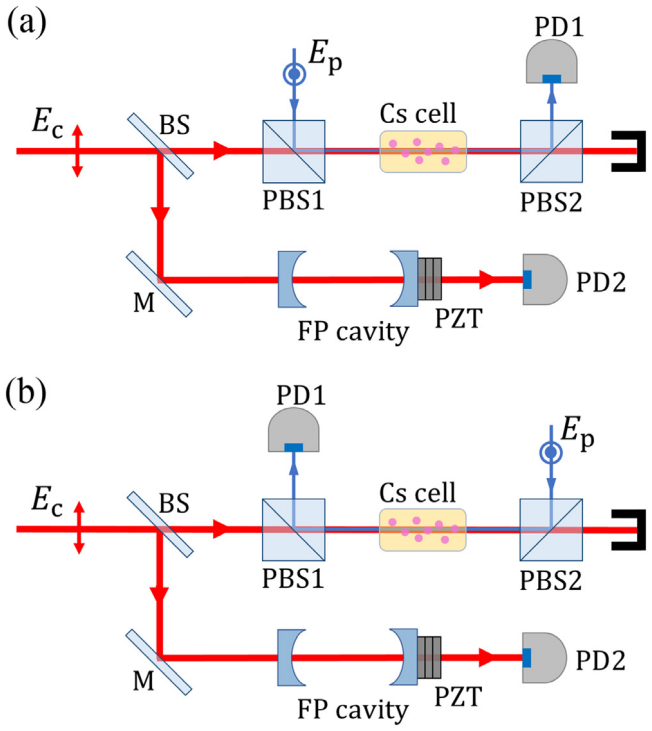


**Fig. 9.** Experimental setup for (a) $\Lambda$- and V-type systems, and (b) UC- and LC-type systems. BS: beam splitter; PBS1, 2: polarization beam splitters; M: reflection mirror; FP cavity: Fabry–Perot cavity; PD1, 2: photodetectors; PZT: Piezoelectric transducer.

$E_{c(p)} = \mathcal{E}_{c(p)} e^{-i\nu_{c(p)}t - i\phi_{c(p)}(t)}$. The phase $\phi_{c(p)}(t)$ undergoes diffusion:

$$\dot{\phi}_{c(p)}(t) = \mu_{c(p)}(t), \tag{11}$$

where $\phi_{c(p)}(0)$ is uniformly distributed between 0 and $2\pi$, and $\mu_{c(p)}(t)$ is a $\delta$-correlated Gaussian stochastic process with

$$\langle \mu_{c(p)}(t) \rangle = 0, \tag{12a}$$

$$\langle \mu_{c(p)}(t_1)\mu_{c(p)}(t_2) \rangle = 2\kappa_{c(p)}\delta(t_1 - t_2), \tag{12b}$$

$$\langle \mu_c(t_1)\mu_p(t_2) \rangle = 0, \tag{12c}$$

The phase diffusion rate $2\kappa_{c(p)}$ in Eq. (12b) equals to the linewidth of the field. Here we assume that the phase fluctuations of the coupling and probe fields are uncorrelated [see Eq. (12c)], since they are provided by two independent (i.e., phase unlocked) lasers.

In order to see how the phase fluctuations of the fields lead to the dephasing of atoms, we consider the evolution of, e.g., $\rho_{23}$ in $\Lambda$-type system:

$$\dot{\rho}_{23} = -(\gamma_{23} - i\delta_p)\rho_{23} - i\Omega_c e^{-i\phi_c(t)}\rho_{21} + i\Omega_p e^{i\phi_p(t)}\rho_{13}. \tag{13}$$

Introducing the variables: $\tilde{\rho}_{21} = \rho_{21}e^{-i\phi_p(t)}$, $\tilde{\rho}_{13} = \rho_{13}e^{i\phi_c}(t)$, and $\tilde{\rho}_{23} = \rho_{23}e^{i[\phi_c(t) - \phi_p(t)]}$, Eq. (13) becomes

$$\dot{\tilde{\rho}}_{23} = -(\gamma_{23} - i\delta_p)\tilde{\rho}_{23} - i\Omega_c\tilde{\rho}_{21} + i\Omega_p\tilde{\rho}_{13} + i[\mu_c(t) - \mu_p(t)]\tilde{\rho}_{23}. \tag{14}$$

Using the theory of multiplicative stochastic processes [42,43], the average of Eq. (14) is

$$\begin{aligned}\langle \dot{\tilde{\rho}}_{23} \rangle &= -(\gamma_{23} - i\delta_p)\langle \tilde{\rho}_{23} \rangle - i\Omega_c\langle \tilde{\rho}_{21} \rangle + i\Omega_p\langle \tilde{\rho}_{13} \rangle \\ &\quad - \int_0^t \langle [\mu_c(t) - \mu_p(t)][\mu_c(\tau) - \mu_p(\tau)] \rangle d\tau \langle \tilde{\rho}_{23} \rangle \\ &= -(\tilde{\gamma}_{23} - i\delta_p)\langle \tilde{\rho}_{23} \rangle - i\Omega_c\langle \tilde{\rho}_{21} \rangle + i\Omega_p\langle \tilde{\rho}_{13} \rangle,\end{aligned} \tag{15}$$

with the effective decay rate

$$\tilde{\gamma}_{23} = \gamma_{23} + \kappa_c + \kappa_p = \gamma_{23}^{(d)} + \kappa_c + \kappa_p. \tag{16}$$

It is clearly seen from Eq. (16) that the phase fluctuations of the fields result in the atomic dephasing with the dephasing rate of $\kappa_c + \kappa_p$. Using the similar procedure, we obtain all the effective decay rates $\tilde{\gamma}_{ij}$ for the four systems. The expressions of $\eta$ for each system are then obtained:

$$\eta = \frac{\Gamma_{12} + \Gamma_{13}}{4} + \frac{\gamma_{12}^{(d)} - \gamma_{23}^{(d)}}{2} - \frac{\kappa_c}{2}, \qquad \Lambda - \text{type}, \tag{17a}$$

$$\eta = \frac{\Gamma_{12} - \Gamma_{31}}{4} + \frac{\gamma_{12}^{(d)} - \gamma_{23}^{(d)}}{2} - \frac{\kappa_c}{2}, \qquad \text{UC} - \text{type}, \tag{17b}$$

$$\eta = -\frac{\Gamma_{31}}{4} + \frac{\gamma_{12}^{(d)} - \gamma_{23}^{(d)}}{2} - \frac{\kappa_c}{2}, \qquad \text{V} - \text{type}, \tag{17c}$$

$$\eta = \frac{\Gamma_{13}}{4} + \frac{\gamma_{12}^{(d)} - \gamma_{23}^{(d)}}{2} - \frac{\kappa_c}{2}, \qquad \text{LC} - \text{type}. \tag{17d}$$

Therefore, the value of $\eta$ and thus the quantum interference can be manipulated by simply adjusting the linewidth of the coupling field $2\kappa_c$, which is much more feasible in practice than controlling the collisional dephasing rate $\gamma_{12(23)}^{(d)}$. In the following experiment, we tune $2\kappa_c$ to show the modulation of quantum interference.

## 3. Experiment

To verify the results in Section 2, we perform an experiment in a 50-mm-long $^{133}$Cs vapor cell. The experimental setup is illustrated in Fig. 9. We use two external-cavity diode lasers (TOPTICA DL Pro) as the coupling and probe fields. For $\Lambda$- and V-type systems, the wavelengths of the two fields are both 895 nm. For UC- and LC-type systems, the wavelength of the coupling (probe) field is 921 nm (852 nm) and 852 nm (921 nm), respectively. The free-running linewidths of the two lasers are about $2\pi \times 1$ MHz. The linewidth $2\kappa_c$ of the coupling laser is controlled by modulating its driving current with a wide-band ($2\pi \times 30$ MHz) white noise from a waveform generator (KEYSIGHT 33500B). A Fabry–Perot (FP) cavity is used to monitor the linewidth. Its finesse and linewidth are measured to be about 450 and $2\pi \times 3$ MHz, respectively. We found that with increase of the noise current (rms) ranging from 0 to 60 μA, the linewidth $2\kappa_c$ can be continuously changed from about

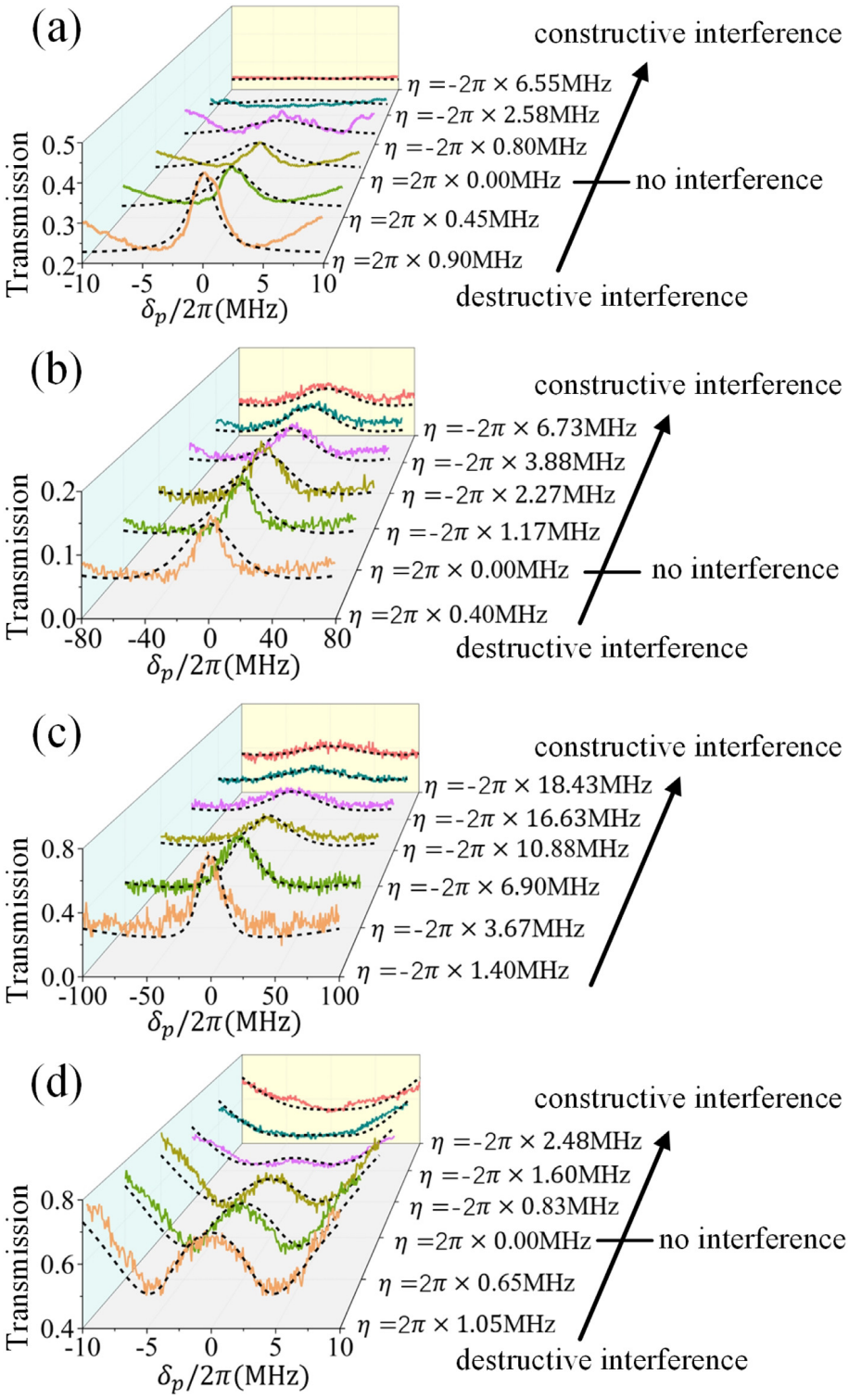


**Fig. 10.** The probe transmission spectra with different values of $\eta$ for (a) $\Lambda$-, (b) UC-, (c) V-, and (d) LC-type systems. The solid and dashed lines represent the experimental data and theoretical calculations, respectively. The Rabi frequencies of the coupling fields are: (a) $\Omega_c = 2\pi\times8.88$ MHz; (b) $\Omega_c = 2\pi\times9.15$ MHz; (c) $\Omega_c = 2\pi\times9.38$ MHz; (d) $\Omega_c = 2\pi\times10.99$ MHz. The vapor temperature $T = 25$ °C. For all the systems, since no buffer gas is filled in the vapor cell, the collisional dephasing rates can be neglected compared to other decay rates, i.e., $\gamma_{12}^{(d)} \approx 0$ and $\gamma_{23}^{(d)} \approx 0$. (For interpretation of the references to color in this figure legend, the reader is referred to the web version of this article.)

$2\pi \times 1$ MHz to over $2\pi \times 70$ MHz. Since the added noise current (0~60 μA) is much smaller than the dc injection current (about 90 mA) driving the laser diode, the current modulation only causes a relative intensity fluctuation (rms) less than 5%. Therefore, for the phase-diffusion model used in Section 2.3, the assumption that the laser field has a stable amplitude and a random phase is still valid even in the presence of the current modulation. In addition, the small intensity modulation to the coupling field has no significant effect on the experimental results. Note that although an external electro-optic phase modulator, such as NEW FOCUS 4006, can be used to modulate the laser phase almost without introducing intensity modulation, we only achieved a linewidth tunable range of $2\pi\times1$ MHz to about $2\pi\times5$ MHz because of its small modulation

depth (about 15 mrad/V). The tunable range is not enough for the present experiment.

The coupling and probe fields with orthogonal polarizations overlap at a polarization beam splitter (PBS), and then pass through the vapor cell in Doppler-free co-propagation ($\Lambda$- and V-type systems) or counter-propagation (UC- and LC-type systems). Afterwards, the probe field is separated from the coupling field by another PBS and detected by a photodetector (PD1). A digital oscilloscope is connected to the photodetector to record the probe absorption spectrum. The vapor cell at room temperature (25 °C) is shielded against external stray magnetic field by three layers of $\mu$-metal. The powers and the $e^{-2}$ full widths of the coupling (probe) field at the cell position are 0.80 mm (0.75 mm) and 300 μW (20 μW), respectively. The frequency of the coupling field is locked at resonance with the transition $|1\rangle \leftrightarrow |3\rangle$, and meanwhile the frequency of the probe field is scanned across the transition $|1\rangle \leftrightarrow |2\rangle$.

Fig. 10 shows the experimental (solid lines) and theoretical (dashed lines) probe transmission spectra with different values of $\eta$. In the theoretical calculation, we consider the Doppler broadening effect arising from the atomic movement by taking the average of the susceptibility: $\chi = \int_{-\infty}^{\infty} \chi(v) f(v) \mathrm{d}v$ with the Maxwell velocity distribution $f(v) = e^{-v^2/u^2}/(\sqrt{\pi}u)$, where $u = \sqrt{2k_\mathrm{B}T/m}$ is the most probable speed of atoms at temperature $T$, $m$ is the atomic mass, and $k_\mathrm{B}$ is the Boltzmann constant.

We precisely adjust the linewidth $2\kappa_\mathrm{c}$ to let $\eta \approx 0$ for each system and refer to this case as the case of no quantum interference, as marked in Fig. 10. For example, in $\Lambda$-type system with $\eta = (\Gamma_{12} + \Gamma_{13})/4 + (\gamma_{12}^{(\mathrm{d})} - \gamma_{23}^{(\mathrm{d})})/2 - \kappa_\mathrm{c}/2$, $\Gamma_{12} = 2\pi \times 3.45$ MHz, $\Gamma_{13} = 2\pi \times 1.92$ MHz, and $\gamma_{12(23)}^{(\mathrm{d})} \ll \Gamma_{13}$, we tune the linewidth of the coupling field $2\kappa_\mathrm{c} = 2\pi \times 5.37$ MHz to get $\eta = 0$. Obviously, when $\eta$ is modulated from positive value to negative value, we observe the transition from suppressed absorption (destructive quantum interference) to enhanced absorption (constructive quantum interference) relative to the case of no quantum interference, as predicted in Section 2. It is to be noted that for V-type system, $\eta$ is always negative [also see Eq. (17c)] and thus the quantum interference is always constructive. From the quantum interference viewpoint, this also explains the well-known fact that for V-type system one cannot obtain a very dip and narrow transparency window [7].

The EIT window becomes smaller and wider when the linewidth $2\kappa_\mathrm{c}$ increases. The further increase of $2\kappa_\mathrm{c}$ to $2\pi \times 15.7$ MHz ($\Lambda$-type system) and $2\pi \times 9.6$ MHz (LC-type system) will leads to the EIT window be vanished [the cyan and pink lines in Fig. 10(a) and (d)]. The wide EIT window modulated by the laser linewidth in a wide range makes it possible to realize broadband light pulse shaping, splitting, and storage.

Due to the Doppler broadening, the atoms may interact with the adjacent hyperfine levels. For $\Lambda$- and V-type systems, the Doppler width $\Delta_\mathrm{D} = 2\nu_\mathrm{p} u\sqrt{\ln 2}/c \approx 2\pi \times 359$ MHz is smaller than the hyperfine-level splittings of $6\mathrm{S}_{1/2}$ ($\Delta\omega_{F=3\leftrightarrow F=4} = 2\pi \times 9.19$ GHz) and $6\mathrm{P}_{1/2}$ ($\Delta\omega_{F'=3\leftrightarrow F'=4} = 2\pi \times 1.17$ GHz), and thus the atoms do not interact with the adjacent hyperfine levels. For UC-type system, the Doppler width $\Delta_\mathrm{D} = 2\pi \times 377$ MHz is comparable to the hyperfine-level splittings of $6\mathrm{P}_{3/2}$ ($\Delta\omega_{F'=4\leftrightarrow F'=5} = 2\pi \times 251$ MHz, $\Delta\omega_{F'=3\leftrightarrow F'=4} = 2\pi \times 201$ MHz, and $\Delta\omega_{F'=2\leftrightarrow F'=3} = 2\pi \times 151$ MHz). Therefore, a small fraction of atoms interacts with the adjacent hyperfine level $|6\mathrm{P}_{3/2}, F' = 4\rangle$. However, due to the Doppler-free configuration, transparency windows corresponding to different hyperfine levels are well separated. Fig. 10(b) only presents the transparency window corresponding to the probe transition $|6\mathrm{P}_{3/2}, F' = 5\rangle \leftrightarrow |6\mathrm{S}_{1/2}, F = 4\rangle$. For LC-type system, the Doppler broadening has little effect on the spectra because the atoms with $kv > \Gamma_{13}$ cannot be efficiently populated to the state $|1\rangle$ to interact with the probe field.

Since the wavelengths of the coupling and probe fields are different, there is some residual Doppler broadening. The residual Doppler width is given by $\delta_\mathrm{D} = \Delta_\mathrm{D}|\nu_\mathrm{c} - \nu_\mathrm{p}|/\nu_\mathrm{p}$. For $\Lambda$- and V-type systems, one has $\delta_\mathrm{D} = 2\pi \times 0.2$ kHz and $2\pi \times 1.6$ kHz, respectively, which are negligible compared to the atomic decay rates. For the two cascade-type systems, one has a relatively large $\delta_\mathrm{D} = 2\pi \times 28$ MHz. The residual Doppler broadening results in a wide transparency window for the UC-type system. However, it fails to broaden the transparency window for the LC-type system because of the near zero population in the state $|1\rangle$ for moving atoms, as analyzed above.

## 4. Conclusions

We have theoretically and experimentally demonstrated the transition between destructive and constructive quantum interference by precisely controlling the dephasing in $\Lambda$-, UC-, V-, and LC-type three-level atomic systems. We have analyzed in detail the effect of dephasing rates on the probe absorption, which can be separated into two Lorentzian terms and a quantum interference term. By adjusting the dephasing rate, the absorption can be suppressed (destructive quantum interference) or enhanced (constructive quantum interference). Due to the difficulty of controlling the collisional dephasing, we have precisely controlled dephasing via adjusting the linewidths of interacting fields, and thus have showed the transition of quantum interference in our experiment.

## Declaration of competing interest

The authors declare that they have no known competing financial interests or personal relationships that could have appeared to influence the work reported in this paper.

## CRediT authorship contribution statement

**Jinhong Liu:** Methodology, Writing - original draft, Data curation. **Jinze Wu:** Conceptualization, Software, Visualization, Methodology. **Yaodong Hu:** Data curation, Validation. **Yu Zhang:** Data curation, Investigation. **Junxiang Zhang:** Conceptualization, Supervision, Funding acquisition, Writing - review & editing.

## Acknowledgment

This work was supported by National Natural Science Foundation of China (91736209, U1330203); National Natural Science Foundation of China (11574188) and Zhejiang Provincial Natural Science Foundation of China (LD18A040001).

## References

[1] Z. Ficek, S. Swain, Quantum Interference and Coherence: Theory and Experiments, Springer New York, 2005.
[2] S.-Y. Zhu, R.C.F. Chan, C.P. Lee, Spontaneous emission from a three-level atom, Phys. Rev. A 52 (1995) 710–716, http://dx.doi.org/10.1103/PhysRevA.52.710.
[3] S.-Y. Zhu, L.M. Narducci, M.O. Scully, Quantum-mechanical interference effects in the spontaneous-emission spectrum of a driven atom, Phys. Rev. A 52 (1995) 4791–4802, http://dx.doi.org/10.1103/PhysRevA.52.4791.
[4] S.-Y. Zhu, M.O. Scully, Spectral line elimination and spontaneous emission cancellation via quantum interference, Phys. Rev. Lett. 76 (1996) 388–391, http://dx.doi.org/10.1103/PhysRevLett.76.388.
[5] M. Fleischhauer, A. Imamoğlu, J.P. Marangos, Electromagnetically induced transparency: Optics in coherent media, Rev. Modern Phys. 77 (2005) 633–673, http://dx.doi.org/10.1103/RevModPhys.77.633.
[6] K.-J. Boller, A. Imamoğlu, S.E. Harris, Observation of electromagnetically induced transparency, Phys. Rev. Lett. 66 (1991) 2593–2596, http://dx.doi.org/10.1103/PhysRevLett.66.2593.
[7] D.J. Fulton, S. Shepherd, R.R. Moseley, B.D. Sinclair, M.H. Dunn, Continuous-wave electromagnetically induced transparency: A comparison of V, $\Lambda$, and cascade systems, Phys. Rev. A 52 (1995) 2302–2311, http://dx.doi.org/10.1103/PhysRevA.52.2302.
[8] J. Gea-Banacloche, Y.-Q. Li, S.-Z. Jin, M. Xiao, Electromagnetically induced transparency in ladder-type inhomogeneously broadened media: Theory and experiment, Phys. Rev. A 51 (1995) 576–584, http://dx.doi.org/10.1103/PhysRevA.51.576.
[9] M. Xiao, Y.-Q. Li, S.-Z. Jin, J. Gea-Banacloche, Measurement of dispersive properties of electromagnetically induced transparency in rubidium atoms, Phys. Rev. Lett. 74 (1995) 666–669, http://dx.doi.org/10.1103/PhysRevLett.74.666.

[10] D.F. Phillips, A. Fleischhauer, A. Mair, R.L. Walsworth, M.D. Lukin, Storage of light in atomic vapor, Phys. Rev. Lett. 86 (2001) 783–786, http://dx.doi.org/10.1103/PhysRevLett.86.783.
[11] B. Julsgaard, J. Sherson, J.I. Cirac, J. Fiurášek, E.S. Polzik, Experimental demonstration of quantum memory for light, Nature 432 (7016) (2004) 482, http://dx.doi.org/10.1038/nature03064.
[12] A.I. Lvovsky, B.C. Sanders, W. Tittel, Optical quantum memory, Nature Photon. 3 (12) (2009) 706, http://dx.doi.org/10.1038/nphoton.2009.231.
[13] Y.F. Hsiao, P.J. Tsai, H.S. Chen, S.X. Lin, C.C. Hung, C.H. Lee, Y.H. Chen, Y.F. Chen, I.A. Yu, Y.C. Chen, Highly efficient coherent optical memory based on electromagnetically induced transparency, Phys. Rev. Lett. 120 (2018) 183602, http://dx.doi.org/10.1103/PhysRevLett.120.183602.
[14] C. Shu, P. Chen, T.K.A. Chow, L.B. Zhu, Y.H. Xiao, M.M.T. Loy, S.W. Du, Subnatural-linewidth biphotons from a Doppler-broadened hot atomic vapour cell, Nature Commun. 7 (2016) 12783, http://dx.doi.org/10.1038/ncomms12783.
[15] L. Zhu, X. Guo, C. Shu, H. Jeong, S. Du, Bright narrowband biphoton generation from a hot rubidium atomic vapor cell, Appl. Phys. Lett. 110 (16) (2017) 161101, http://dx.doi.org/10.1063/1.4980073.
[16] C.F. McCormick, V. Boyer, E. Arimondo, P.D. Lett, Strong relative intensity squeezing by four-wave mixing in rubidium vapor, Opt. Lett. 32 (2) (2007) 178–180, http://dx.doi.org/10.1364/OL.32.000178.
[17] M. Guo, H. Zhou, D. Wang, J. Gao, J. Zhang, S. Zhu, Experimental investigation of high-frequency-difference twin beams in hot cesium atoms, Phys. Rev. A 89 (2014) 033813, http://dx.doi.org/10.1103/PhysRevA.89.033813.
[18] D.-W. Wang, H.-T. Zhou, M.-J. Guo, J.-X. Zhang, J. Evers, S.-Y. Zhu, Optical diode made from a moving photonic crystal, Phys. Rev. Lett. 110 (2013) 093901, http://dx.doi.org/10.1103/PhysRevLett.110.093901.
[19] C. Hu, S.A. Schulz, A.A. Liles, L. O'Faolain, Tunable optical buffer through an analogue to electromagnetically induced transparency in coupled photonic crystal cavities, ACS Photon. 5 (5) (2018) 1827–1832, http://dx.doi.org/10.1021/acsphotonics.7b01590.
[20] J. Wu, J. Zhang, S. Zhu, G.S. Agarwal, Spin–Hall effect of light and its enhancement in multilevel atomic system, Opt. Lett. 45 (1) (2020) 149–152, http://dx.doi.org/10.1364/OL.45.000149.
[21] G.S. Agarwal, S. Huang, Electromagnetically induced transparency in mechanical effects of light, Phys. Rev. A 81 (2010) http://dx.doi.org/10.1103/PhysRevA.81.041803, 041803(R).
[22] S. Marcinkevičius, A. Gushterov, J.P. Reithmaier, Transient electromagnetically induced transparency in self-assembled quantum dots, Appl. Phys. Lett. 92 (4) (2008) 041113, http://dx.doi.org/10.1063/1.2840160.
[23] Z. Dutton, K.V.R.M. Murali, W.D. Oliver, T.P. Orlando, Electromagnetically induced transparency in superconducting quantum circuits: Effects of decoherence, tunneling, and multilevel crosstalk, Phys. Rev. B 73 (2006) 104516, http://dx.doi.org/10.1103/PhysRevB.73.104516.
[24] N. Liu, L. Langguth, T. Weiss, J. Kästel, M. Fleischhauer, T. Pfau, H. Giessen, Plasmonic analogue of electromagnetically induced transparency at the Drude damping limit, Nature Mater. 8 (9) (2009) 758, http://dx.doi.org/10.1038/nmat2495.
[25] N. Gisin, R. Thew, Quantum communication, Nature Photon. 1 (3) (2007) 165, http://dx.doi.org/10.1038/nphoton.2007.22.
[26] E. Knill, R. Laflamme, G.J. Milburn, A scheme for efficient quantum computation with linear optics, Nature 409 (6816) (2001) 46, http://dx.doi.org/10.1038/35051009.
[27] S.H. Autler, C.H. Townes, Stark effect in rapidly varying fields, Phys. Rev. 100 (1955) 703–722, http://dx.doi.org/10.1103/PhysRev.100.703.
[28] C.N. Cohen-Tannoudji, The Autler–Townes effect revisited, in: R.Y. Chiao (Ed.), Amazing Light: A Volume Dedicated to Charles Hard Townes on His 80th Birthday, Springer New York, 1996, pp. 109–123, http://dx.doi.org/10.1007/978-1-4612-2378-8_11.
[29] J. Wu, J. Liu, Y. He, Y. Zhang, J. Zhang, S. Zhu, Quantum interference manipulation and enhancement with fluctuation-correlation-induced dephasing in an atomic system, Phys. Rev. A 98 (4) (2018) 043829, http://dx.doi.org/10.1103/PhysRevA.98.043829.
[30] P.M. Anisimov, J.P. Dowling, B.C. Sanders, Objectively discerning Autler–Townes splitting from electromagnetically induced transparency, Phys. Rev. Lett. 107 (2011) 163604, http://dx.doi.org/10.1103/PhysRevLett.107.163604.
[31] L. Giner, L. Veissier, B. Sparkes, A.S. Sheremet, A. Nicolas, O.S. Mishina, M. Scherman, S. Burks, I. Shomroni, D.V. Kupriyanov, P.K. Lam, E. Giacobino, J. Laurat, Experimental investigation of the transition between Autler–Townes splitting and electromagnetically-induced-transparency models, Phys. Rev. A 87 (2013) 013823, http://dx.doi.org/10.1103/PhysRevA.87.013823.
[32] B. Peng, Ş.K. Özdemir, W. Chen, F. Nori, L. Yang, What is and what is not electromagnetically induced transparency in whispering-gallery microcavities, Nature Commun. 5 (2014) 5082, http://dx.doi.org/10.1038/ncomms6082.
[33] H.-C. Sun, Y.-X. Liu, H. Ian, J.Q. You, E. Il'ichev, F. Nori, Electromagnetically induced transparency and Autler–Townes splitting in superconducting flux quantum circuits, Phys. Rev. A 89 (2014) 063822, http://dx.doi.org/10.1103/PhysRevA.89.063822.
[34] L.-Y. He, T.-J. Wang, Y.-P. Gao, C. Cao, C. Wang, Discerning electromagnetically induced transparency from Autler–Townes splitting in plasmonic waveguide and coupled resonators system, Opt. Express 23 (18) (2015) 23817–23826, http://dx.doi.org/10.1364/OE.23.023817.
[35] H.-C. Li, G.-Q. Ge, H.-Y. Zhang, Dressed-state realization of the transition from electromagnetically induced transparency to Autler–Townes splitting in superconducting circuits, Opt. Express 23 (8) (2015) 9844–9851, http://dx.doi.org/10.1364/OE.23.009844.
[36] J. Liu, J. Wu, Y. Zhang, Y. He, J. Zhang, Influence of dephasing on the Akaike-information-criterion distinguishing of quantum interference and Autler–Townes splitting in coherent systems, J. Opt. Soc. Amer. B 37 (1) (2020) 49–55, http://dx.doi.org/10.1364/JOSAB.37.000049.
[37] E. Saglamyurek, T. Hrushevskyi, A. Rastogi, K. Heshami, L.J. LeBlanc, Coherent storage and manipulation of broadband photons via dynamically controlled Autler–Townes splitting, Nature Photon. 12 (12) (2018) 774, http://dx.doi.org/10.1038/s41566-018-0279-0.
[38] E.E. Mikhailov, I. Novikova, Y.V. Rostovtsev, G.R. Welch, Buffer-gas-induced absorption resonances in Rb vapor, Phys. Rev. A 70 (2004) 033806, http://dx.doi.org/10.1103/PhysRevA.70.033806.
[39] A. Sargsyan, D. Sarkisyan, U. Krohn, J. Keaveney, C. Adams, Effect of buffer gas on an electromagnetically induced transparency in a ladder system using thermal rubidium vapor, Phys. Rev. A 82 (2010) 045806, http://dx.doi.org/10.1103/PhysRevA.82.045806.
[40] T.Y. Abi-Salloum, Electromagnetically induced transparency and Autler–Townes splitting: Two similar but distinct phenomena in two categories of three-level atomic systems, Phys. Rev. A 81 (2010) 053836, http://dx.doi.org/10.1103/PhysRevA.81.053836.
[41] S. Davuluri, Y. Wang, S. Zhu, Destructive and constructive interference in the coherently driven three-level systems, J. Modern Opt. 62 (13) (2015) 1091–1097, http://dx.doi.org/10.1080/09500340.2015.1020895.
[42] G.S. Agarwal, Quantum statistical theory of optical-resonance phenomena in fluctuating laser fields, Phys. Rev. A 18 (1978) 1490–1506, http://dx.doi.org/10.1103/PhysRevA.18.1490.
[43] R.F. Fox, Contributions to the theory of multiplicative stochastic processes, J. Math. Phys. 13 (8) (1972) 1196–1207, http://dx.doi.org/10.1063/1.1666123.